Monthly Notices of the ROYAL ASTRONOMICAL SOCIETY

MNRAS 496, 5149–5159 (2020) doi:10.1093/mnras/staa1839
Advance Access publication 2020 June 26

Abnormal scattering event in the direction to the pulsar B0834+06

T. V. Smirnova,[1★] V. I. Shishov,[1] A. S. Andrianov,[2★] M. S. Burgin,[2] E. N. Fadeev,[2] M. V. Popov,[2] A. G. Rudnitskii,[2] V. A. Soglasnov[2] and V. A. Zuga[2]

[1]Pushchino Radio Astronomy Observatory, Astro Space Center, Lebedev Physical Institute, Russian Academy of Sciences, Pushchino, Moscow oblast' 142290, Russia
[2]Astro Space Center, Lebedev Physical Institute, Russian Academy of Sciences, Profsoyuznaya str 84/32, Moscow 117997, Russia

Accepted 2020 June 19. Received 2020 June 19; in original form 2019 September 2

ABSTRACT

Analysis of Space-VLBI observations of the pulsar B0834+06 conducted with RadioAstron at 324 MHz shows that in some cases one of the scattering screens could be located very close to the pulsar (about 10 pc from the pulsar), and it has a strong influence on the secondary spectra. For this case, the vertices of inverted arcs are aligned along the main parabolic arc and their width is inversely proportional to the scattering time. The shape of the main arc is determined by another scattering screen that is located at a distance of about 210 pc from the pulsar. The position of this screen is observed to be stable during 19 yr and its spatial scale is larger than 5.6×10^{15} cm. We found that the scattering disc may be approximated by an ellipse with a 2.5 axial ratio and with the position angle of the major axis of about -8°. A small-scale structure with a size of 0.1 au located at the close to observer screen and very high electron density of tens to a few thousand cm^{-3} for different models can be responsible for arclets in a secondary spectra. Additionally, angular refraction exists in the direction towards the pulsar. That suggests the presence of the cosmic prism. We have estimated the angle of refraction to be $\theta_{\rm ref} > 2$ mas and the distance from prism to the observer $D < 160$ pc.

Key words: ISM: general – ISM: structure – pulsars: individual: RadioAstron B0834+06.

1 INTRODUCTION

Pulsar observations provide a powerful tool to study the properties of interstellar plasma in the different directions of the Galaxy. Pulsar radio emission propagating through the interstellar medium is affected by the scattering on the inhomogeneities of the electron density. This leads to many observable effects: angular broadening, temporal broadening of pulses, the frequency and time modulation of the radio emission intensity with the characteristic frequency and time-scales. The study of these effects allows us to investigate the spatial structure of the electron density inhomogeneity of the interstellar plasma.

A large volume of pulsar experimental data has been interpreted in the context of homogeneous isotropic Kolmogorov turbulence in a wide range of scales (Rickett 1990; Armstrong, Rickett & Spangler 1995; Shishov & Smirnova 2002). However, in recent years a number of works indicated the existence of the compact ionized structures in the ISM with a significant impact on the scattering of pulsar radio emission (Stinebring et al. 2001; Hill et al. 2003; Smirnova et al. 2014; Popov et al. 2016; Shishov et al. 2017). It was shown that for some directions the spectral index n of inhomogeneities significantly differs from the Kolmogorov $n = 11/3$. In particular, values $n \approx 3$ were found in the direction to the pulsars: B0950+08 (Smirnova et al. 2014), B0834+06, B1237+25, and B2016+28 (Fadeev et al. 2018). Up to now, there is no theoretical interpretation of such kind of turbulent plasma spectra. Observations also demonstrate the importance of 'cosmic prisms' – large-scale transverse gradients of plasma column density on the lines of sight to several nearby pulsars (Smirnova et al. 2014; Shishov et al. 2017).

Scintillation arcs were first detected by Stinebring et al. (2001) in the secondary spectra (SS). The SS is the squared modulus of the 2D Fourier transform of the dynamic spectrum in the delay (conjugate to frequency) and fringe rate (conjugate to time) domain. The usual interpretation of scintillation arcs is that the main parabola corresponds to the interference of the emission between the scattered rays and the direct ray. The inverted arclets are caused by the interference of waves contained within the normal scattering disc with a faint halo of waves scattered at much larger angles (Cordes et al. 2006). Pen & Levin (2014) suggested that the arclets arise when observed radiation intersects the reconnection sheets in the interstellar plasma nearly aligned with the line of sight.

Here, we present our approach to the interpretation of observations of scattered radiation with space-ground VLBI observations.

Very long baselines (up to 330 000 km) in space-ground VLBI observations with RadioAstron provide an opportunity to obtain a high angular resolution of up to 1 mas at the meter wavelengths (92 cm), and thus to measure the scattering angle $\theta_{\rm H}$ directly.

2 OBSERVATIONS AND DATA ANALYSIS

The pulsar PSR B0834+06 is one of the brightest pulsars in a broad frequency range. According to Liu et al. (2016), the distance to the pulsar is $R = 0.62 \pm 0.06$ kpc. At this distance the proper motion measured with a high accuracy by Lyne, Anderson & Salter (1982)

★ E-mail: tania@prao.ru (TVS); andrian@asc.rssi.ru (ASA);

Table 1. Parameters of observation and data reduction.

Epoch	T, min	Ground Telescopes	b, 10^3 km	Number of channels	Positional angle φ, deg
26.04.2012	120	AR	202.0–205.0	65 536	-16 ± 0.4
08.12.2014	60	GB	63.0–64.0	2048	
08.04.2015	95	AR, GB, WB	147.0–152.0	65 536	22.6 ± 0.3
09.01.2018	120	AR	82.5	2048	-88.3 ± 0.6
24.02.2018	120	AR	75.0	2048	2 ± 0.4
24.11.2018	120	AR	171.5	2048	47 ± 0.6

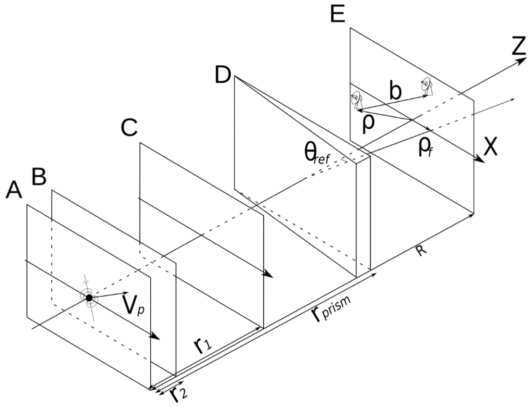

Figure 1. Scattering screens and 'cosmic prism' revealed in the direction of the pulsar: A – object plane, B – anomalous temporary scattering screen, C – main permanent scattering screen, D – cosmic prism, and E – observer plane. Meaning of various designations used on the figure is explained in the text.

implies a transverse velocity of $V_\alpha = 6 \pm 15\,\mathrm{km\,s^{-1}}$, $V_\delta = 151^{+15}_{-06}$ $\mathrm{km\,s^{-1}}$ corresponds to tangential velocity $|\boldsymbol{V}_\mathrm{p}| = 150 \pm 20\,\mathrm{km\,s^{-1}}$.

Observations of PSR B0834+06 were carried out with RadioAstron space-ground interferometer at 324 MHz. Signal was recorded in the band 316–332 MHz. The following ground telescopes participated in the observations: Arecibo (AR), Westerbork (WB), and Green Bank (GB). Table 1 presents the dates, duration of observations, T, baseline projections of the space-ground interferometer, b, the number of spectral channels used for the correlation, and position angle, φ, for cosmic baselines for different epochs. The description of data processing and analysis can be found in Fadeev et al. (2018).

Auto and cross-spectra $I(\boldsymbol{\rho}, \boldsymbol{\rho}+\boldsymbol{b}, f, t)$ were calculated by software ASC CORRELATOR (Likhachev et al. 2017) using on-pulse gating mode and incoherent dedispersion. Here, $\boldsymbol{\rho}$ – the spatial coordinate in the observer plane perpendicular to the line of sight, $\boldsymbol{b}$ – the base of interferometer, f – frequency, and t – time. For definition of $I(\boldsymbol{\rho}, \boldsymbol{\rho}+\boldsymbol{b}, f, t)$ see equation (A1). The duration of on-pulse and off-pulse gates was chosen at the level of 10 per cent of the maximum intensity in average profile. On-pulse and off-pulse spectra were averaged over four pulsar periods. In our further analysis, we used dynamic spectra – moduli of autospectra and cross-spectra.

Interpretation of observational results revealed several layers of plasma on the line of sight to the pulsar contributing to the formation of observed scintillation pattern. The overall picture of the relevant plasma structures on the line of sight is illustrated in Fig. 1. Here we present our model.

The pulsar emission propagating along the z-axis directed to the Earth passes in succession through three layers of interstellar plasma that influence observed statistical properties of received radiation. First, it encounters two scattering layers B and C located, correspondingly, at distances r_2 and r_1 from the pulsar. The scattering layers are considered to be statistically uniform phase screens. Scattering by the screens does not change average direction of the rays.

Then, the rays pass through the cosmic prism D located at the distance r_prism from the pulsar. The prism does not randomly scatter the radiation, but changes the direction of a ray by angle θ_ref. Due to deflection, the intersection of the ray with the observer plane E shifts by vector $\boldsymbol{\rho}_f$, which is parallel to the x-axis relative to the intersection of the ray undeflected by the prism. Deflection angle, θ_ref, and, consequently, displacement $\boldsymbol{\rho}_f$ depends on frequency f.

The model qualitatively outlined here is described in more details in the Appendix A, where relationships between physical parameters of the scattering and refracting layers and observable quantities are derived.

2.1 Dynamic spectra, structure functions, and scintillation scales

Here, we continue the analysis of our data for PSR 0834+06 obtained from observations of 2012–2015 (Fadeev et al. 2018) and also present the new data from observations of 2018. Dynamic spectra of the pulsar are presented on the left-hand side of Figs 2 and 3 in logarithmic scale for intensity. We recorded data without calibration so we cannot perform astrometry analysis of our data and do not present here interferometric phase. Large-scale oblique structures in SS are clearly visible in all our measurements except for 2012 data. In 2012 observations only diffractive structures with much smaller frequency and time-scales were observed.

Diffractive spots are extended along the line $f = (\mathrm{d}f/\mathrm{d}t)t$. Such drift indicates the refraction caused by a cosmic prism in the direction to the pulsar. We determined the drift rate of the diffractive structure by calculating the position of a maximum of the average cross-correlation function between spectra separated in time with the step of $4mP_1$, where $m = 1, 2, \ldots$ and P_1 is the pulsar period. We found the slope $\mathrm{d}f/\mathrm{d}t = 0.77\,\mathrm{kHz\,s^{-1}}$ for 08.04.2015 and $\mathrm{d}f/\mathrm{d}t = 1.34\,\mathrm{kHz\,s^{-1}}$ for 08.12.2014.

Fig. 4 shows the frequency (the filled squares) and time (the open squares) structure functions (SF) for 08.04.2015 (AR–GB baseline) in the log–log scale. These SFs were obtained from frequency–time correlation functions. Fitting by the power law gives $\alpha_1 = 1.19 \pm 0.03$ (time SF) and $\alpha_2 = 1.13 \pm 0.01$ (frequency SF). The errors correspond to fitting uncertainties. That the slopes are nearly the same for time and frequency SFs implies that the scintillation may be described by the refractive model (Shishov et al. 2003). Analysis of SFs for other days supports this conclusion.

The time and frequency scintillation scales, the power index of inhomogeneities spectrum $n = \alpha + 2$, the scale of the diffraction pattern in the observer plane ρ_dif, and the amplitude of visibility function B_u are presented in Table 2. All these parameters and also the parameter of curvature a from analysis of SS, relative distances

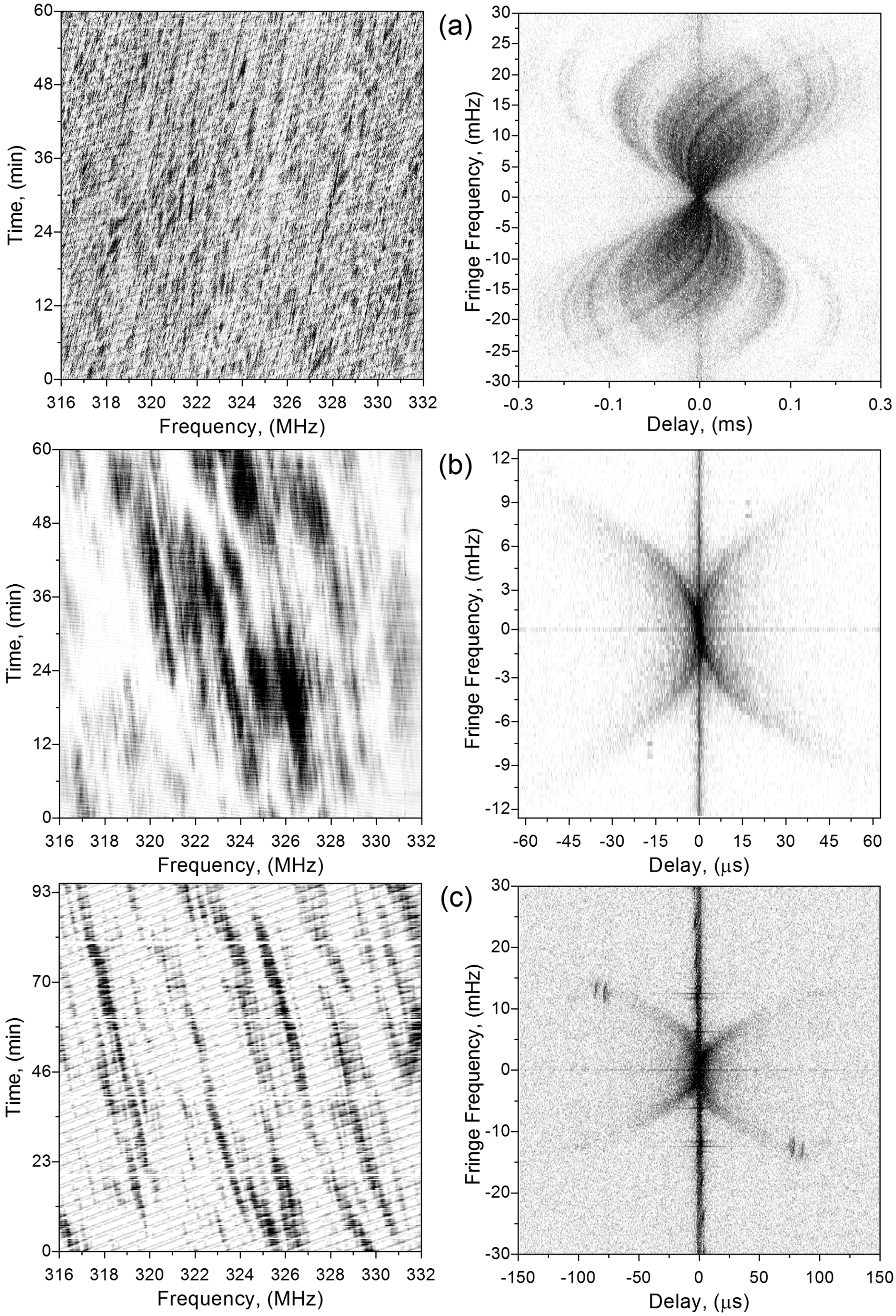

Figure 2. From top to bottom: dynamic spectra (left) and the secondary spectra (right) of PSR B0834+06 for 26.04.2012 (a, autospectra, Aresibo), 08.12.2014 (b, autospectra, Green Bank) and 08.04.2015 (c, cross-spectra, Aresibo – Green Bank) observations correspondingly. Logarithmic scale for intensity was used for dynamic and secondary spectra.

r_1/R (r_1 is a distance from the pulsar to the screen) and scattering angle for 2012–2015 were obtained in (Fadeev et al. 2018). In this paper, we present new data for 2018, and a model explaining our data. We detect refraction in the direction to pulsar and suggest a possible interpretation of spots in the SS for observing dates 2015 April 8 09.02018 January. Values of $\rho_{\rm dif}$ and B_u were obtained from analysis of the normalized covariation function from complex cross-spectra for the RadioAstron-Arecibo baseline (equations A2–

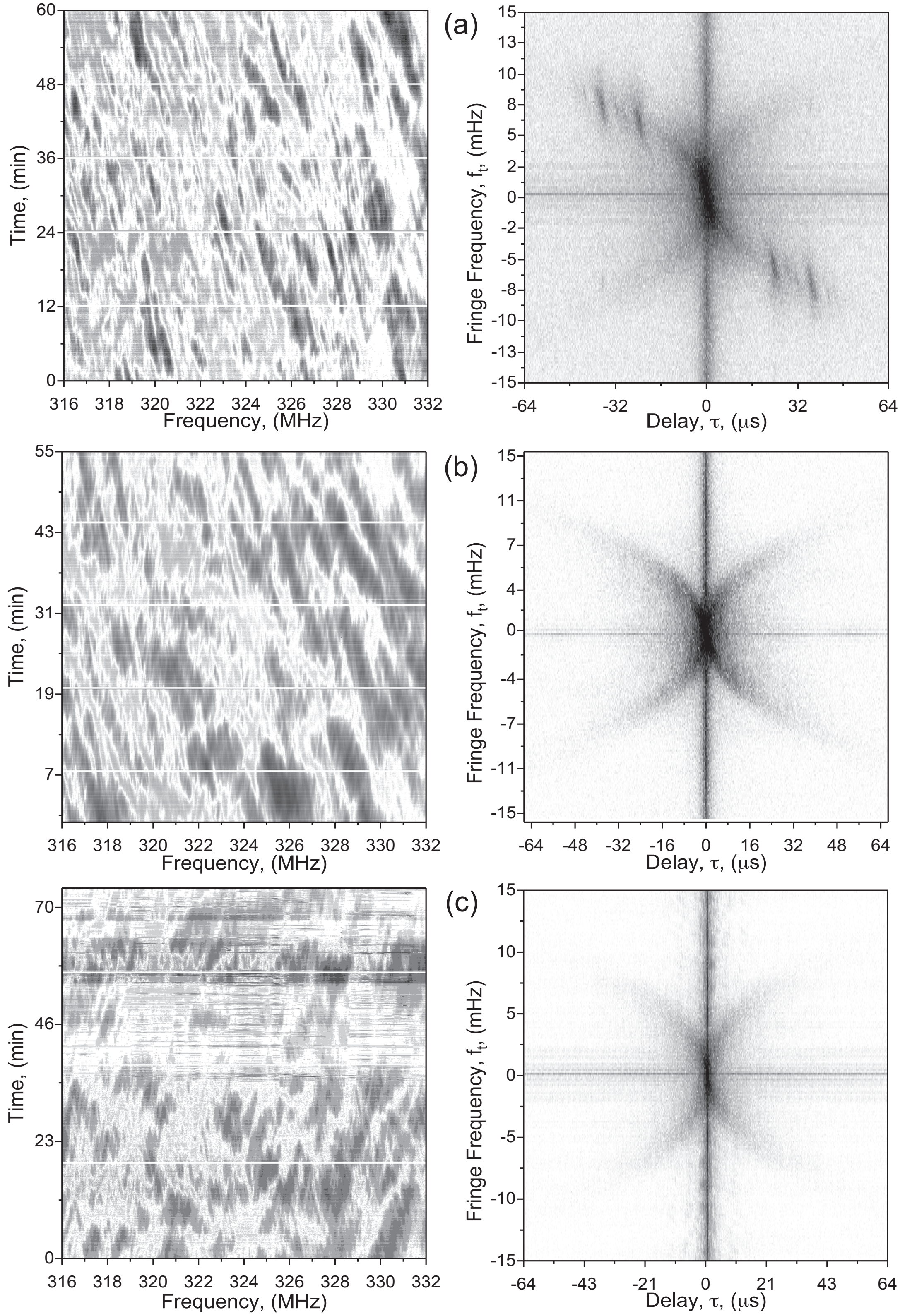

Figure 3. From top to bottom: dynamic spectra (left) and the secondary spectra (right) of PSR B0834+06 for 09.01.2018 (a, autospectra, Aresibo), 24.02.2018 (b, autospectra, Aresibo), and 24.11.2018 (c, autospectra, Aresibo) observations correspondingly. Logarithmic scale for the intensity was used for dynamic and secondary spectra.

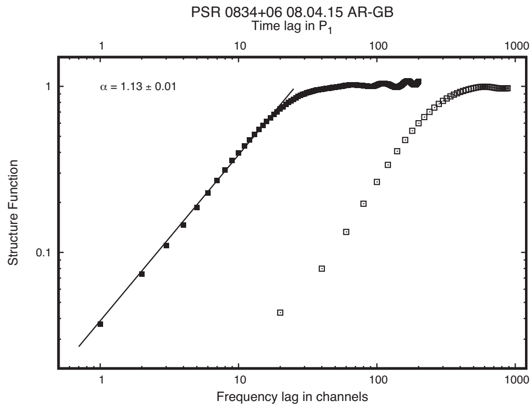

Figure 4. The frequency (the black squares, bottom x-axis, frequency resolution $\Delta f = 15.625$ kHz) and time (the white squares, top x-axis) structure functions for Arecibo – Green Bank baseline are shown in the log–log scale.

A5). The scale $\rho_{\rm dif}$ was determined from

$$B_u(\boldsymbol{b}) = \exp\left[-\frac{1}{2}\left(\frac{|\boldsymbol{b}|}{\boldsymbol{\rho}_{\rm dif}}\right)^{\alpha}\right], \qquad (1)$$

where $\alpha = n - 2$. For dates 2014 Decemeber 8 and 2018 November 24, we did not have a cosmic base and also had a lot of interference, so we could not determine structure and covariation functions reliably and calculate n, $\rho_{\rm dif}$, and B_u. Here, we measure the scale $\boldsymbol{\rho}_{\rm dif}$ in the direction of the baseline for each day of observation.

In the presence of refraction, the power index γ in the dependence diffractive scale versus frequency should be $f_{\rm dif} \sim f^{\gamma}$, where $\gamma = 2 + n/(n-2) = 4.77$ for $n = 3.13$ (Smirnova & Shishov 2008). This dependence is shown in double logarithmic scale in Fig. 5. We present our measurements at 324 and 112 MHz (observations of 2012–2018 at 324 MHz – the white squares, at f = 112 MHz – asterisks). Observation at 112 MHz was carried out in Pushchino Radio astronomy Observatory in 2012 with a frequency resolution of 0.625 kHz. We measured $f_{\rm dif} = 3$ kHz. We also show here data points taken from the literature (the references are given in the caption of Fig. 5). The best fit of measurements by the power law gives the slope $\gamma = 4.7 \pm 0.3$, which corresponds to the expected one. For Kolmogorov spectrum ($n = 11/3$) γ should be equal to 4.2 in the presence of refraction.

The distance from the pulsar to the permanent scattering layer, r_1, was obtained from comparison of the spatial and time-scales of scintillation (see Table 2). For a thin phase screen model the following relationship holds:

$$V_x t_{\rm dif}(R - r_1)/r_1 = \rho_{\rm dif}\cos\mu, \qquad (2)$$

where μ is the angle between scattering axis and the direction of baseline and V_x is a component of the velocity vector parallel to the direction of scattering ($V_x = V_{\rm p}\cos\beta$). Here, we assume that the velocity of the pulsar (151 km s^{-1}) is much larger than the velocities of the screen (10–20 km s^{-1}) and the observer ($\sim$30 km s^{-1}).

2.2 The size and direction of the diffraction pattern

We have measured the characteristic scales of the diffraction pattern $\boldsymbol{\rho}_{\rm dif}$ in different epochs. The results are listed in Table 2.

Our definition of $\boldsymbol{\rho}_{\rm dif}$ is based on analysis of covariation function expressed in equation (1). This value defines the characteristic spatial scale of inhomogeneities responsible for the scattering of emission. For each day, we have different directions of baselines and the value of $\boldsymbol{\rho}_{\rm dif}$ in these directions. Fig. 6 shows the scattering ellipse where $\boldsymbol{\rho}_{\rm dif}$ is placed according to the position angle of each baseline. The position angles, φ, for cosmic baselines for different epochs are listed in Table 1. For the pulsar velocity $\varphi = 2 \pm 6°$ and it is shown in the centre of the figure. For observation of 2018 February 24, the baseline direction is almost perpendicular to the pulsar velocity and the baseline for 2018 January 9. The ratio of the main axes is about 2.5. The position angle of the major axis of our ellipse is $-8°$. We are sure that we have the same scattering disc as in many previous observations (also in Brisken et al. 2010), and so we can use the positional angle of the main scattering axis $-25°$ measured by Brisken et al. (2010) for our calculations. In this case, we have for projection of pulsar velocity $V_x = V_{\rm p}\cos\beta = 134.5$ km s^{-1}, where $\beta = 27°$ is the angle between pulsar velocity and scattering axis. Using equation (2) and the value of $\mu = 25° + \varphi$, we can recalculate r_1/R for all dates (in Fadeev et al. 2018, r_1/R was defined for $\beta = 0$ and $\mu = 0$). These values are listed in the Table 2 with upper index 'cov'. The mean value (excluding 2012 data) is $\langle r_1/R\rangle = 0.37 \pm 0.05$ and the distance from observer to the screen is 390 ± 60 pc, which is very close to the value determined from previous observations.

Using our estimates made at different epochs, we determine the shape of the scattering disc. It reflects the central part of SS, where the main power of scattered emission is located. Brisken et al. (2010) investigate the spatial distribution of scintillation power associated with interference between pairs of points on the scattering disc. This power in SS included in arc structure has just a few per cent of the whole power. Obtained modest anisotropy of the central part of the scattered image using our data does not contradict to a strong anisotropy observed by Brisken et al. (2010) for the scattering screen.

2.3 Secondary spectra

The SS for 2012–2018 shown in Figs 2 and 3 (right-hand side) consist of two components: the central bright component M_1 and the weak component M_2, which is distributed along the parabolic arc.

The component M_1 is a featureless oblique elliptic spot at the centre. Its major axis is oriented along the direction $\tau = ({\rm d}t/{\rm d}f)f_t$, which is its slope that corresponds to the slope of features in the dynamic spectra. The extent of the first component in the direction of the line $\tau_1 = ({\rm d}t/{\rm d}f)f_t$ is much larger than to the direction $f_t = const$. This indicates that the projections to the celestial sphere of the pulsar velocity and the vector $\boldsymbol{\rho}_{\rm f}$ describing the displacement of the scintillation pattern due to cosmic prism are approximately parallel.

The second component M_2 of the SS is concentrated near the arc with $\tau = af_t^2$, where a is a curvature parameter. Points distributed along the main arc correspond to the interference between a highly scattered component and the components arising near the bright centroid (Cordes et al. 2006). The component M_2 originates from the diffraction of radiation on a phase screen with 1D inhomogeneities as it is described in the Appendix A. Fadeev et al. (2018) found that $a = 0.57 \pm 0.05$ µs mHz^{-2} for 2012–2015 data. The relative distance from the pulsar to the scattering screen was calculated from the arc parameter a (see equation A17):

$$Rr_1/(R - r_1) = 2acV_{\rm p}^2\cos^2\beta/\lambda^2. \qquad (3)$$

Relative distances r_1/R with upper index 'arc' and parameter of the arc curvature a are shown in Table 2. Here, we used $\beta = 27°$, $V_{\rm p} = 151$ km s^{-1}, and $R = 0.62$ kpc.

Brisken et al. (2010) observed PSR B0834+06 at four frequency bands including our 324 MHz. They defined the main arc by the curvature $a = 5.577 \cdot 10^{16}/f^2$(s^3) (here f is the centre frequency

Table 2. Scattering parameters at 324 MHz. Columns are as follows: date of observations, scintillation time $t_{\rm dif}$, decorrelation bandwidth $f_{\rm dif}$, power index of inhomogeneities spectrum n, spatial scale of the diffraction pattern $\rho_{\rm dif}$, amplitude of visibility function B_u, relative distances r_1/R measured using covariation function (upper index cov) and secondary spectra (upper index arc), curvature parameter a.

Epoch	$t_{\rm dif}$, s	$f_{\rm dif}$, kHz	n	$\rho_{\rm dif}$, 10^9 cm	B_u	$(r_1/R)^{\rm cov}$	$(r_1/R)^{\rm arc}$	a, μs mHz^{-2}
26.04.2012	12 ± 2	4.0 ± 0.5	2.83 ± 0.04	9.3 ± 0.9	0.38 ± 0.09	0.017 ± 0.004	0.27 ± 0.09	0.56 ± 0.03
08.12.2014	314 ± 10	350 ± 20	–	–	–	–	0.27 ± 0.09	0.57 ± 0.03
08.04.2015	220 ± 15	210 ± 10	3.13 ± 0.01	6.0 ± 0.9	0.25 ± 0.04	0.42 ± 0.06	0.3 ± 0.1	0.58 ± 0.05
09.01.2018	190 ± 10	185 ± 10	3.03 ± 0.02	4.1 ± 0.4	0.40 ± 0.06	0.4 ± 0.06	0.28 ± 0.09	0.58 ± 0.03
24.02.2018	240 ± 20	280 ± 15	3.10 ± 0.03	8.9 ± 1.5	0.68 ± 0.01	0.29 ± 0.06	0.29 ± 0.09	0.62 ± 0.02
24.11.2018	170 ± 20	235 ± 20	–	–	–	–	0.29 ± 0.09	0.62 ± 0.01

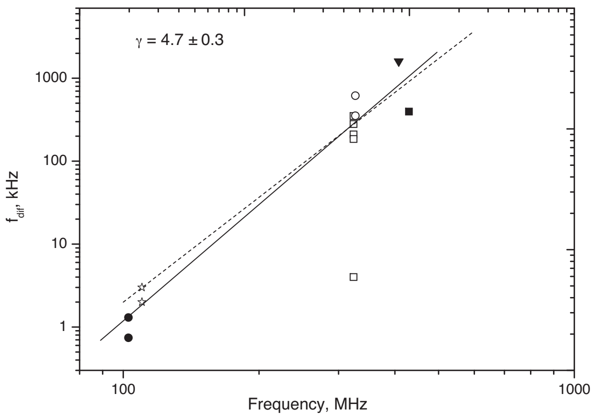

Figure 5. Decorrelation bandwidth of scintillation versus the observation frequency in log–log scale: the white squares correspond to our observations at 324 MHz, the white asterisks – 112 MHz; the black circles – (Smirnova 1992); the white circles – (Bhat, Rao & Gupta 1999), the black squares – (Cordes, Wiseberg & Boriakof 1985), and the triangle – (Smith & Wright 1985). The outlier value $f_{\rm dif} \approx 4.0$ kHz for observations at 324 MHz corresponds to observations of the year 2012. The solid line with a slope $\gamma = 4.7 \pm 0.3$ shows the best fit of experimental data (with the outlier excluded) by the power law. The dashed line corresponds to Kolmogorov spectrum with $\gamma = 4.2$.

in Hz) that for f = 322.5 MHz (the centre frequency of one of the bands) corresponds to $a = 0.536\ \mu$s mHz^{-2}. This value agrees with our results within the error. We can see from Table 2 that r_1/R obtained from covariation function is about 20 per cent larger than determined from the arc structure. However, these two different definitions depend on $V_{\rm p}$ and R with its own errors and so this difference can be not substantial.

2.4 Refraction

Our results can be explained by the diffraction of the emission on the phase screen and differential angular refraction after the scattered emission passes through the cosmic prism. The frequency structure of scintillation of the emission passed through the cosmic prism is determined by the refractive displacement of the diffraction pattern with frequency. If the characteristic value of the refraction angle $\theta_{\rm ref}$ is much greater than the characteristic value of the $\theta_{\rm dif}$, then the fine frequency structure of scintillation is determined by the refractive relative displacement of beam paths at two frequencies that causes rearrangement of speckles of the diffractive scintillation pattern that changes with frequency. Let we have a cosmic prism, located close to the observer at a distance of $R - r_{\rm prism}$, which deflects the beam at frequency f, then the difference in refraction angle at a nearby frequency $f + \Delta f$ is $\Delta\theta_{\rm ref} = 2\Delta f/f \cdot \theta_{\rm ref}$ equation (A8), where $\theta_{\rm ref}$ is a shift of source position visible in the observer plane at frequency f. Here, $r_{\rm prism}$ is a distance from pulsar to prism. We assume that the frequency scale of the pattern $f_{\rm dif}$ is less than the offset of the scattering from refraction then we obtain that the displacement:

$$2(f_{\rm dif}/f)(R - r_{\rm prism})\theta_{\rm ref} < \rho_{\rm dif}. \quad (4)$$

Using determined values of $f_{\rm dif}$ and $\rho_{\rm dif}$ (Table 2) for 2015 data we obtain

$$\theta_{\rm ref} < 0.88(R - r_1)/(R - r_{\rm prism})\ [\rm mas]\,. \quad (5)$$

In deriving equation (A16), we ignored the influence of the angular refraction caused by the cosmic prism. This effect leads to a shift of parabola in coordinate f_t. For the same values of τ the branches with positive and negative values of f_t are shifted by the same value of $\delta f_t = 0.4 \pm 0.2$ MHz for 2014 and $\delta f_t = 0.9 \pm 0.3$ MHz for 2015. Value δf_t is determined by the refraction angle. If the cosmic prism is located close to the observer, $(R - r_{\rm prism}) \ll R$, then $\theta_{\rm ref}$ and δf_t are connected by the relation

$$\theta_{\rm ref} = R\lambda\delta f_t/[(R - r_1)V_{\rm p}\cos\beta]\,. \quad (6)$$

We assume here that the directions of $V_{\rm p}$ and $\theta_{\rm ref}$ are approximately parallel because we see strongly elongated features from diffraction spots in the dynamic spectra. Using $\delta f_t = 0.9 \pm 0.3$ MHz and $r_1/R = 0.42 \pm 0.06$, and taking into account relation (5) we obtain $\theta_{\rm ref} = 2.0 \pm 0.6$ mas/cos β and

$$R - r_{\rm prism} < (160 \pm 60)\cos\beta\ [\rm pc]. \quad (7)$$

So the distance from the observer to the prism is less than 160 ± 60 pc and $\theta_{\rm ref} > 2.0 \pm 0.6$ mas. For $\beta = 27^\circ$, we have $\theta_{\rm ref} = 2.2$ mas and $R - r_{\rm prism} = 140$ pc.

2.5 Analysis of 2012 observations

Scintillation parameters for 2012 observations (Table 2) strongly differ from the parameters for 2014–2018. Scintillation time-scale and decorrelation bandwidth differ by more than order of magnitude from the corresponding values for other dates. The mean frequency autocorrelation function (frequency resolution is 244 Hz) is shown in Fig. 7(a). The measured decorrelation bandwidth, $f_{\rm dif} = 4 \pm 0.5$ kHz at 324 MHz, lies significantly lower than the value predicted by the relation $f_{\rm dif}(f)$ shown in Fig. 5.

This significant decrease in frequency and time-scales is very rare event. Bhat, Cordes & Chatterjee (2003) carried out monitoring of this pulsar during 930 d and did not see such event. The distance to the scattering screen from the observer, $d_{\rm s}$, was determined in (Fadeev et al. 2018) by comparing the spatial and the time-scale equation (2): $d_{\rm s} = R - r_2 = 0.6 \pm 0.1$ kpc. The screen is located very close to the pulsar: $d_{\rm s}/R = 0.98$, $r_2 = 12 \pm 2$ pc. Including angles

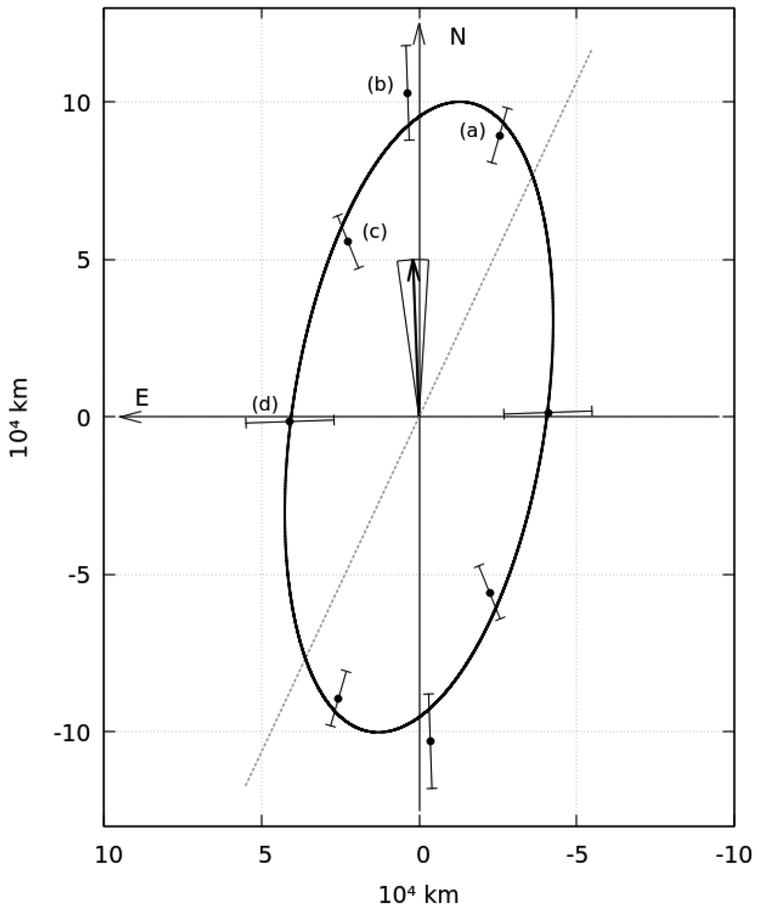

Figure 6. Scattering ellipse obtained from measuring the spatial scale ρ_{dif} with different orientations of the baseline: (a) observation of 26.04.2012, (b) 24.02.2018, (c) 08.04.2015, and (d) 09.01.2018. The position angle of the pulsar velocity is shown by the arrow at the centre. The positional angle of the main scattering axis determined in Brisken et al. (2010) is shown by the dashed line.

μ and β in equation (2) we get $r_2 = 10.5$ pc. Independent estimate of d_{s} using the measured value of the scattering time $\tau_{\mathrm{sc}} = 8 \pm 1\,\mu$s and the relation $d_{\mathrm{s}} = R[\theta_H^2 R/(8c\tau_{\mathrm{sc}} \ln 2) + 1]^{-1}$ (Britton, Gwinn & Ojeda 1998), where θ_H is the angular diameter of the scattering disc, gave the same value of d_{s}. The scattering time was estimated from the dependence of visibility function amplitude versus delay shown in Fig. 7(b).

The SS for 2012 is shown in Fig. 2(a). It consists of a dense set of thin arclets that goes up to 0.3 ms. The vertices of these arclets are lying along the main arc having the same parameter of curvature within the errors $a = 0.56 \pm 0.03\ \mu\mathrm{s\,mHz^{-2}}$ as for 2014, 2015, and 2018. These arclets are observed for the case when the emission that is strongly scattered by the screen located close to the pulsar at a distance of $r_2 = 12 \pm 2$ pc falls on the screen with 1D inhomogeneities located at a mean distance $r_1 = 210 \pm 40$ pc from the pulsar defined from two methods. So two screens exist on this date. The screen closest to the pulsar produces the scattering angle of 45 mas. This value corresponds to the strong scattering mode.

3 DISCUSSION

3.1 Distribution of scattering material in the direction to pulsar

The results of our study can be explained by the existence of two scattering screens and a prism located on the line of sight from the observer to the pulsar (see Fig. 1). The scattering screen, which is located at the distance of $r_1 = 210 \pm 40$ pc from the pulsar, dominates the scintillation in the observations of 2014–2018. The spatial scale ρ_{dif} and the time-scale t_{dif} of scintillation are formed there. This screen is also responsible for the arc structure observed in the SS.

A cosmic prism is located between this screen and the observer at a distance less or about 160 pc from the observer. There are a few results pointing to the existence of angular refraction in the direction to PSR B0834+06: the drift of diffractive spots in the dynamic spectra, the same slope of the frequency and time SFs, the dependence of frequency scale of scintillation on the frequency of observation. Differential refraction on the prism converts the spatial structure of scintillation to the frequency scintillation with a scale of 200–300 kHz. Bhat et al. (1999) carried out monitoring of scintillation parameters of PSR B0834+06 between 1993 and 1995, spanning 930 d. The average values of frequency and time-scales were measured to be $t_{\mathrm{dif}} = 300$ s and $f_{\mathrm{dif}} = 400$ kHz. These parameters are close to values obtained for the 2014–2018 observations presented in this paper. However, these parameters show variations with a time-scale of about 10 d as was mentioned in Bhat et al. (1999). The possible reason for these variations could be an influence of the refractive scintillations on the diffractive ones (Blandford & Narayan 1985; Shishov 1995).

The drift of diffractive spots is often observed in the dynamic spectra of this pulsar. This effect is also caused by the refraction of the scattered emission on the cosmic prism. The prism was observed

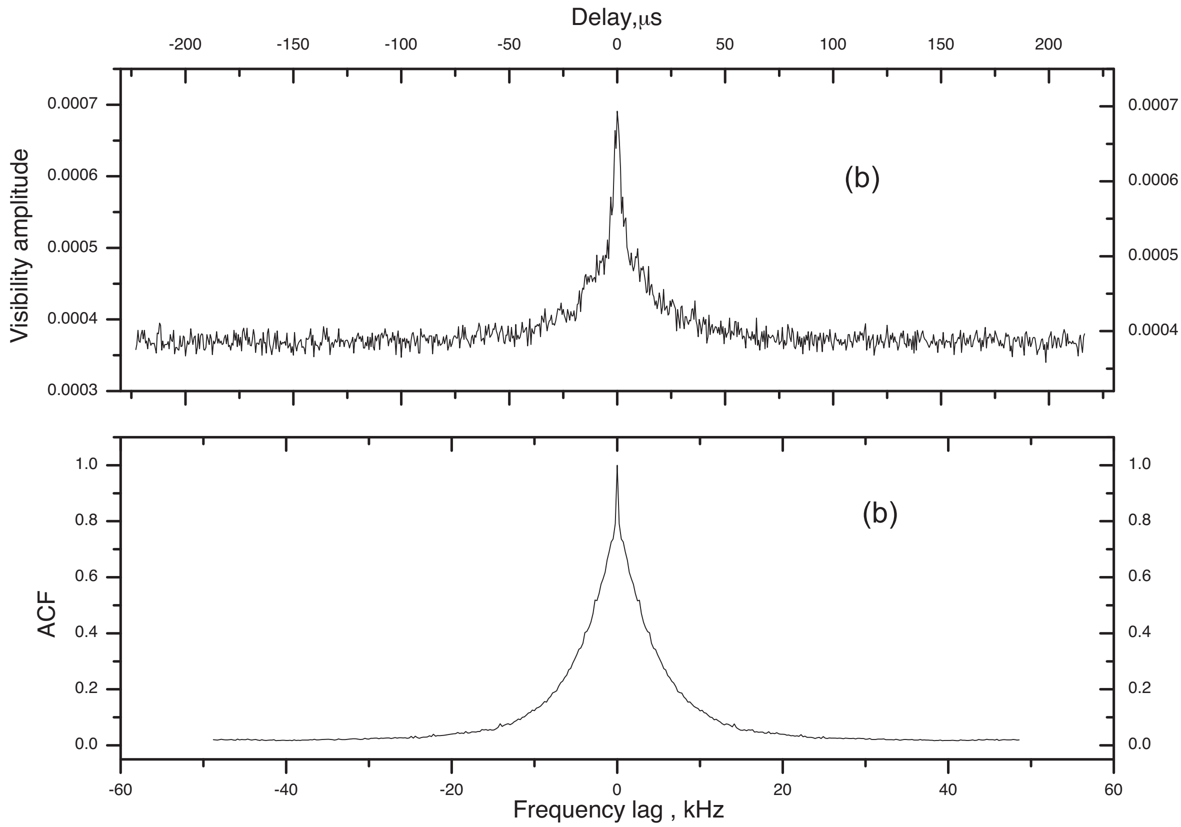

Figure 7. (a) The mean frequency autocorrelation function versus frequency lag; (b) dependence of visibility function amplitude versus delay.

for a long time, although the angle between the direction of refraction and pulsar velocity varies. These directions were nearly parallel in 2014 and 2015. Bhat et al. (1999) claimed that for PSR B0834+06 persistent drift slopes exist over a few months. There have been many observations of PSR B0834+06 in the last two decades mainly aimed to study the SS and arc structure (Stinebring et al. 2001; Hill et al. 2003; Brisken et al. 2010). The distance from the observer to the scattering screen determined from the known distance to the pulsar and the parabola curvature parameter a is about 420 pc. This value remains constant for a long time starting between 1999 (Stinebring et al. 2001) and 2018 (measurements presented in this paper). Thus, the spatial scale of this screen should be larger than 5.6×10^{15} cm.

Observations of 2012 indicate the existence of two scattering screens. One of them is a strong scattering layer of turbulent plasma at a distance of only **12 ± 2** pc ($r_2/R = 0.02$) from the pulsar, and another has a stable location with a distance of $r_1 = 210 \pm 40$ pc from the pulsar. The time of crossing the line of sight by this close screen is less than 19.5 months (2012–2014), so its spatial scale is less than $S = 7.5 \times 10^{14}$ cm. The appearance of this layer on the line of sight is a rare event. Brisken et al. (2010) observed PSR B0834+06 on 2005 November 12 and used the same frequency resolution (244 Hz) of the dynamic spectra for the data analysis. They pointed out that the decorrelation bandwidth of scintillation on this day was 3 kHz, which is close to our estimate (4 kHz). It is possible that they also observed an additional scattering layer located close to the pulsar. The most bright details in their SS are observed at delays up to about 300−350 μs (Fig. 1 Brisken et al. 2010) as for our data presented in Fig. 2(a). The details for the delay scales of 1 ms are not visible in our observation, but we think that the structures up to 300 μs are caused by the screen closest to the pulsar.

Table 3. Scattering parameters: fringe frequency f_t, the angular position of the observed details in the secondary spectra θ, their spatial locations from the centre of the image δs, and the radius of the scattering disc θ_{sc}.

Epoch	f_t, MHz	θ, mas	δs, 10^{13}, cm	θ_{sc}, mas
08.04.2015	12.5; 13.1	8.2; 8.6	4.9; 5.1	0.5 ± 0.75
09.01.2018	6.15; 7.23	4.1; 4.8	2.4; 2.8	0.34 ± 0.12

3.2 Discrete structures in the main arc

Two isolated details located at the main parabola are seen in the SS for 2015 April 8 and 2018 January 9 observations. These details correspond to the narrow bandwidth fringes observed in the dynamic spectrum. According to the model of scintillation arcs (Stinebring et al. 2001; Cordes et al. 2006), it can be explained as a result of interference between rays scattered at a bright spot on the image periphery and the image centre. The measured fringe frequency, f_t, for 2015 and for 2018 January 9 of these details are presented in Table 3. It is possible to estimate the angular separation between the points at the central region ($\theta \approx 0$) and another point in the image plane oriented along the direction of the effective pulsar velocity. The relation for the angular separation of points in the image plane is given in equation (A15): $\theta = r\lambda f_t/[(R - r)V_p] = \lambda f_t/V_{eff}$, where $V_{eff} = V_p(R - r)/r$ and r is a distance from the pulsar to the screen. For $R = 0.62$ kpc, $r/R = 0.34 \pm 0.06$ and $V_{eff} = 290$ km s^{-1} the angular position of the observed details, θ, their spatial locations from the centre of the image, δs, and the radius of the scattering disc, θ_{sc}, are shown in the Table 3. Here θ_{sc} is defined as

$$\theta_{sc} = \lambda(2\pi\rho_{dif})^{-1} . \quad (8)$$

The value of f_t for each arclet we defined as the mean position of points with amplitudes exceeding three times the mean amplitude of the noise in SS. The accuracy of f_t is approximately 5 per cent.

The separation between these structures is only 0.07 au for 2015 April 8 and 0.13 au for 2018 January 9. The fine-scale substructure exists on the distances much greater than the size of the scattering disc. We did not observe these structures 4 months earlier in 2014 and after 46 d from 2018 January 9, when the line of sight shifted by $\approx(0.38-1)\times 10^{14}$ cm.

Four isolated arclets for PSR B0834+06 were observed in 2004 over 3 weeks (Hill et al. 2005). These arclets are scattered within the values of 7−12 mas that is close to the scales measured in this paper. It was shown that arclets are caused by stationary structures in the scattering screen. These arclets can be caused by discrete structures similar to those responsible for extreme scattering events (ESEs) such as plasma lens (Coles et al. 2015). As it was shown in Brisken et al. (2010), the scattering responsible for each arclet originates at a location that is independent of wavelength. It can be if the arclet were caused by a lens-like concentration of plasma, and the waves are deflected at a fixed transverse distance from the pulsar line of sight. The angular size of such a lens should be small and its angular position is much larger than the size of the scattering disc. We have $\theta/\theta_{\rm sc} > 12$ in our case (Table 3).

Walker & Wardle (1998) proposed a model for explaining ESEs in the quasar 0954+658 where radio wave refraction is due to ionized material generated by the photoevaporation of an underlying neutral hydrogen cloud traversing the line of sight. The electron density at the surface of the cloud is given by $n_{\rm e} = 4.87\times 10^9/D^{0.5}$, where D is a cloud radius in cm and $n_{\rm e}$ in cm^{-3}. For a cloud radius 1 au electron density will be $n_{\rm e}\approx 10^3$ cm^{-3}. The presence of such a cloud on the line of sight will cause fourfold enhancement in intensity of the image, and it may lead to the formation of two or four arclets in the SS. For 09.01.18 we see four arclets, two of them are weak. We can evaluate the size of lens as $s\approx\Delta\theta(1-r/R)R/2$, where $\Delta\theta$ is an angular separation between two more brighter arclets. For $\Delta\theta = 0.7$ mas the size is $s = 3.3\times 10^{12}$ cm or about 0.1 au. For such small clouds $n_{\rm e}$ should be about 3000 cm^{-3}. This electron density is much more than the average $n_{\rm e}$ in the warm diffuse interstellar medium which is 0.5 cm^{-3}.

Clegg et al. (1998) presented description of the refractive properties of an interstellar 1D Gaussian plasma lens. Using this model, Hill et al. (2005) evaluated an average electron density in lens as $\langle n_{\rm e}\rangle = (5.4\,{\rm cm}^{-3})\theta/\lambda^2$, where the wavelength λ is expressed in meters, the angular position θ in mas and get $\langle n_{\rm e}\rangle\approx 100\,{\rm cm}^{-3}$. In our case, we have for $\theta = 4$ mas, $\langle n_{\rm e}\rangle = 25\,{\rm cm}^{-3}$ (09.01.2018) and for $\theta = 8.6$ mas, $\langle n_{\rm e}\rangle = 54\,{\rm cm}^{-3}$ (08.04.2015). This model predicts caustic surfaces and in the region between the inner and outer caustics an observer would see the undeflected image of the source and two deflected subimages. In this case, Hill et al. (2005)

$$\langle n_{\rm e}\rangle = \frac{1.9\,{\rm cm}^{-3}\,\alpha\,\Delta\theta/(1\,{\rm mas})}{\lambda^2/(1\,{\rm m})^2}, \qquad (9)$$

where α is the refractive strength parameter and λ in m. We have the ratio of the peak power of the arclet to the power in the centre of SS: $l = 0.037$. Using $l = 1/(1+\alpha)$ and $\Delta\theta = 0.7$ mas, we get $\langle n_{\rm e}\rangle\approx 40.9$ cm $^{-3}$ (2018 January 9).

Existence of close inverts arcs can be explained by preliminary modulation of emission on the screen located close to the pulsar before being scattered on the main screen. The main arc is not very pronounced in the SS obtained from 2012 data where we observe the wide distribution of power for inverted arclets. The width of the strip in the direction of f_t is almost 20–25 times higher than the width of arcs for 2014 and 2015 observation. This ratio of widths corresponds to the inverse ratio of the time diffractive scales for these dates 210, 350, and 12 s. As discussed in the Appendix, the characteristic width of this strip in the direction of f_t is approximately equal to $\Delta f_t\approx 1/(2\pi t_{\rm dif})$.

4 CONCLUSIONS

Scattering angle, temporal broadening, frequency, and time-scales of scintillation were measured for five epochs of VLBI observations (2012, 2014, 2015, and 2018) for the pulsar B0834+06 at 324 MHz with the space-ground interferometer RadioAstron. Analysis of these measurements enables us to estimate the distances to the effective scattering screens. We find that there is a permanent (for all epochs) screen, located at a distance of 210 ± 40 pc from the observer, which is approximately 2/3 of the distance to the pulsar. The scattering of the pulsar radio emission on this screen leads to the formation of parabolic arcs in the SS. The distance to the screen determined by the curvature of parabolic arcs coincides with the value determined by a comparison of the scattering angle and the temporal broadening. Measuring of the visibility function for different projections of the cosmic baselines on the pulsar velocity vector (different epochs) permits us to determine the shape of the scattering disc. It is an ellipse with an axial ratio of 2.5 and with the position angle of the major axis being about -8°. The small anisotropy of this ellipse does not contradict strong anisotropy observed by Brisken et al. (2010), who showed that the main image was highly elongated. The shape of our ellipse reflects the central part of SS, where the main power of the scattered emission is located. Data presented here show that dense compact refractors can be responsible for a separate arclets in SS. Plasma inhomogeneities that appeared on the line of sight in this case are similar to those that caused ESEs observed for extragalactic radio sources (Fiedler et al. 1994; Coles et al. 2015). Refraction effects manifested by the slope of diffraction spots in the dynamic spectra indicate the presence of the cosmic prism located at a distance less than 160 pc from the observer with a refraction angle exceeding 2 mas.

For 2012 epoch an anomalous scattering is observed. Scattering parameters (decorrelation bandwidth, temporal broadening, characteristic scintillation time) differ several dozen times from the values of 2014–2018 epochs. The distance of the anomalous scattering screen from the pulsar is about 10 pc or approximately 1/50 of the distance between the pulsar and the observer. The scattering of radio emission at such close to the pulsar distance results in an anomalously large scattering angle of about 45 mas. The presence in the SS of parabolic arcs with the same value of curvature as for other epochs indicates the existence of the stable screen for 2012 epoch. In this case, the main arcs are accompanied by the multiple inverted arclets that might be formed because of the scattering on the screen located close to the pulsar.

ACKNOWLEDGEMENTS

The RadioAstron project is led by the Astro Space Center of the Lebedev Physical Institute of the Russian Academy of Sciences and the Lavochkin Scientific and Production Association under a contract with the Russian Federal Space Agency, in collaboration with partner organizations in Russia and other countries.

We are very grateful to the staff at the Westerbork synthesis array for their support.

Partly based on observations with the Green Bank Observatory, which is a facility of the National Science Foundation operated under cooperative agreement by Associated Universities, Inc.

The Arecibo Observatory is operated by SRI International under a cooperative agreement with the National Science Foundation (AST-1100968) and in alliance with Ana G. Mendez-Universidad Metropolitana and the Universities Space Research Association.

This work was supported by the Russian Foundation for Basic Research (project code 16-02-00954).

Facility: RadioAstron Space Radio Telescope (Spektr-R), GBT (Green Bank Observatory), WSRT (Westerbork synthesis array), and Pushchino 22-m radio telescope, used as Tracking Station.

DATA AVAILABILITY

The data underlying this article will be shared on reasonable request to the corresponding author.

REFERENCES

Armstrong J. W., Rickett B. J., Spangler S. R., 1995, ApJ, 443, 209
Bhat N. D. R., Rao A. P., Gupta Y., 1999, ApJS, 121, 483
Bhat N. D. R., Cordes J. M., Chatterjee S., 2003, ApJ, 584, 782
Blandford R., Narayan R., 1985, MNRAS, 213, 591
Brisken W. F., Mackquart J.-P., Gao J. J., Rickett B. J., Coles W. A., Deller A. T., Tingay S. J., West C. J., 2010, ApJ, 708, 232
Britton M. C., Gwinn C. R., Ojeda M. J., 1998, ApJ, 501, L101
Clegg A. W., Fey A. L., Lazio T., Joseph W., 1998, ApJ, 496, 253
Coles W. A. et al., 2015, ApJ, 808, 113
Cordes J. M., Wiseberg J. M., Boriakof V., 1985, ApJ, 288, 221
Cordes J. M., Rickett B. J., Stinebring D. R., Coles W. A., 2006, ApJ, 637, 346
Fadeev E. N. et al., 2018, MNRAS, 480, 4199
Fiedler R., Dennison B., Johnston K. J., Waltman E. B., Simon R., 1994, ApJ, 430, 581
Hill A. S., Stinebring D. R., Barnor H. A., Berwick D. E., Webber A. B., 2003, ApJ, 599, 457
Hill A. S., Stinebring D. R., Asplund C. T., Berwick D. E., Everett W. B., Hinkel N. R., 2005, ApJ, 619, L171
Likhachev S. F., Kostenko V. I., Girin I. A., Andrianov A. S., Rudnitskiy A. G., Zharov V. E., 2017, J. Astron. Instrum., 6, 1750004
Liu S., Pen U.-L., Macquart J.-P., Brisken W., Deller A., 2016, MNRAS, 458, 1289
Lyne A. G., Anderson B., Salter M. J., 1982, MNRAS, 201, 503
Pen U. L., Levin Y., 2014, MNRAS, 442, 3338
Popov M. V. et al., 2016, Astron. Rep., 60, 792
Prokhorov A. M., Bunkin V. F., Gochelashvily K. S., Shishov V. I., 1975, Proc. IEEE, 63, 790
Rickett B. J., 1990, A&A, 28, 561
Shishov V. I., 1976, Radiophys. Quantum Electron, 19, 1056
Shishov V. I., 1995, Waves Random Media, 5, 497
Shishov V. I., Smirnova T. V., 2002, Astron. Reports, 46, 731
Shishov V. I. et al., 2003, A&A, 404, 557
Shishov V. I., Smirnova T. V., Gwinn C. R., Andrianov A. S., Popov M. V., Rudnitskiy A. G., Soglasnov V. A., 2017, MNRAS, 468, 3709
Smirnova T. V., 1992, Sov. Astron. Lett., 18, 392
Smirnova T. V., Shishov V. I., 2008, Astron. Rep., 52, 736
Smirnova T. V. et al., 2014, ApJ, 786, 115
Smith F. G., Wright N. C., 1985, MNRAS, 214, 97
Stinebring D. R., McLaughlin M. A., Cordes J. M., Becker K. M., Goodman J. E. E., Kramer M. A., Sheckard J. L., Smith C. T., 2001, ApJ, 549, L97
Walker M., Wardle M., 1998, ApJ, 498, L125

APPENDIX A: THEORETICAL RELATIONS

Quasi-instantaneous interferometric response with the baseline $\boldsymbol{b}$ (cross-spectrum of the field) is defined as

$$\begin{aligned} I(\boldsymbol{\rho}, \boldsymbol{\rho}+\boldsymbol{b}, f, t) &= \langle E(\boldsymbol{\rho}, f, t) E^{*}(\boldsymbol{\rho}+\boldsymbol{b}, f, t)\rangle \\ &= H(f, t) j(\boldsymbol{\rho}, \boldsymbol{\rho}+\boldsymbol{b}, f, t), \end{aligned} \tag{A1}$$

where $E(\boldsymbol{\rho}, f, t)$ is a spectrum of the field propagated through the turbulent interstellar plasma, $H(f, t)$ is a flux defined by the pulsar, $\boldsymbol{\rho}$ – the spatial coordinate in the observer plane perpendicular to the line of sight, $\boldsymbol{b}$ – the base of interferometer and f, t – frequency and time. Let the mean flux of pulsar, $\langle H(f, t)\rangle = 1$, $j(\boldsymbol{\rho}, \boldsymbol{\rho}+\boldsymbol{b}, f, t)$ is a component of the response of the interferometer, defined by the interstellar medium. It is a random function of $\boldsymbol{\rho}$, $\boldsymbol{b}$, f, and t parameters.

Analysis of the observational data is based on the approaches used in Smirnova et al. (2014) and Shishov et al. (2017). Multiplying $I(\boldsymbol{\rho}, \boldsymbol{\rho}+\boldsymbol{b}, f, t)$ by its complex conjugate in frequency $f+\Delta f$ and averaging over time and frequency, one can obtain for the regime of strong scintillations (Prokhorov et al. 1975):

$$\begin{aligned} J_1(\boldsymbol{b}, \Delta f) &= |\langle j(\boldsymbol{\rho}, \boldsymbol{\rho}+\boldsymbol{b}, f, t) j^{*}(\boldsymbol{\rho}, \boldsymbol{\rho}+\boldsymbol{b}, f+\Delta f)\rangle| \\ &= |B_u(\Delta f)|^2 + |B_u(\boldsymbol{b})|^2). \end{aligned} \tag{A2}$$

Here, $B_u(\boldsymbol{b})$ – the spatial field-coherence function with a single average flux in the observer's plane, $B_u(\Delta f)$ is the frequency covariation function of flux fluctuations, it does not depend on the baseline. $|B_u(\boldsymbol{b})|^2$ can be obtained by calculating the normalized covariation function:

$$J_1(\boldsymbol{b}, \Delta f \gg f_{\rm dif})/J_1(\boldsymbol{b}, \Delta f = 0) = |B_u(\boldsymbol{b})|^2/(1+|B_u(\boldsymbol{b})|^2), \tag{A3}$$

where $f_{\rm dif}$ is a decorrelation bandwidth of scintillation. The spatial field-coherence function is defined by (Prokhorov et al. 1975)

$$B_u(\boldsymbol{\rho}) = \exp(-D_{\rm s}(\boldsymbol{\rho})/2), \tag{A4}$$

where $D_{\rm s}(\boldsymbol{\rho})$ is a spatial SF of phase fluctuations. For the power spectrum of the electron density inhomogeneities with index n, the SF also has a power-law form

$$D_{\rm s}(\boldsymbol{\rho}) \sim |\boldsymbol{\rho}|^{n-2}. \tag{A5}$$

For the case of the simplest model of the phase screen located at a distance r from the pulsar

$$D_{\rm s}(\boldsymbol{\rho}) = D_{S,1}((r/R)\boldsymbol{b}), \tag{A6}$$

where $D_{S,1}(\rho)$ is the phase SF for the radiation outgoing from the phase screen, R is the distance from the pulsar to the observer. If the transverse velocity of the pulsar is $\boldsymbol{V}_{\rm p}$, then point of intersection of line of sight with the screen moves relative to the plasma with velocity

$$\boldsymbol{V}_1 = [(R-r)/R]\boldsymbol{V}_{\rm p}. \tag{A7}$$

Here, we assume that V_1 is much greater than the velocities of the observer and the screen.

In the presence of cosmic prism located close to the observer, the frequency structure of the scintillation pattern is determined by the frequency-dependent angular deflection of the diffraction pattern by the prism (Shishov et al. 2003). This prism deflects the beam with an angle of refraction $\Delta\theta_{\rm ref}$. If $\theta_{\rm ref}$ is the resulting shift of source position in the observer plane at frequency f, then the difference in refraction angle at a nearby frequency $f+\Delta f$ is (Shishov et al. 2003) $\Delta\theta_{\rm ref} = 2\theta_{\rm ref}\Delta f/f$. Linear displacement of the pattern in the observer plane is given by

$$|\boldsymbol{\rho}_f| = 2(\Delta f/f)(R - r_{\rm prism})\theta_{\rm ref}, \tag{A8}$$

where $r_{\rm prism}$ is a distance from the pulsar to the prism, $\theta_{\rm ref}$ is an angle of refraction, f – the frequency of observation.

Let us consider the phase screen with 1D inhomogeneities of phase fluctuations (in the direction of x-axis). The arc structures in the SS are formed after the propagation of the emission through this screen. Resulting field correlation function that corresponds to the small values of ρ_x (less than coherence scale) is

$$B_u(\rho_x) = \exp[-(1/2)D_{\rm s}(\rho_x)] \approx 1 - (1/2)D_{\rm s}(\rho_x)\,, \tag{A9}$$

where ρ_x is a projection of $\boldsymbol{\rho}$ on x-axis. In the observer plane $B_u(\Delta f, \rho_x)$ is defined as (Shishov 1976)

$$B_u(\Delta f, \rho_x) \approx 1 - \frac{1}{2}\int {\rm d}\rho_x' G(r, \Delta f, \rho_x - \rho_x') D_{\rm s}[(r/R)\rho_x'], \tag{A10}$$

where

$$G(r, \Delta f, \rho_x - \rho_x') = \left(\frac{kr}{4\pi i k_1 R(R-r)}\right)^{1/2} \times \exp\left(-\frac{kr(\rho_x - \rho_x')^2}{4ik_1 R(R-r)}\right), \tag{A11}$$

$k_1 = \Delta k/2k = \Delta f/2f$, $k = 2\pi/\lambda$. We introduce 2D Fourier transform from $B_u(\Delta f, \rho_x)$ as

$$M_u(\tau, \theta_x) = \int {\rm d}\Delta f \int {\rm d}\rho_x \exp(-i2\pi\Delta f\tau - ik\theta_x\rho_x) \times B_u(\Delta f, \rho_x). \tag{A12}$$

Here, $k\theta_x$ is the spatial frequency, θ_x – scattering angle, τ is the delay conjugate to frequency. For large τ and θ_x, the equation (A12) will be

$$M_u(\tau, \theta_x) \approx (1/2)\delta\left(\tau - A\theta_x^2\right)\Phi_{S,1}[(R/r)k\theta_x]. \tag{A13}$$

Here, $A = r(R - r)/2cR$, $\delta(\tau - A\theta_x^2)$ – delta function, $\Phi_{S,1}$ is the spectrum of electron density inhomogeneities.

If V_x is a projection of the pulsar velocity on the x-axis, then the velocity of motion of the diffraction pattern in the observer plane is

$$\boldsymbol{V}_x = \boldsymbol{\rho}_{\rm dif} r/(R-r)t_{\rm dif}, \tag{A14}$$

where $\boldsymbol{\rho}_{\rm dif}$ and $t_{\rm dif}$ are the spatial and the time-scales of scintillation. The spatial frequency $q_x = k\theta_x$ is connected with a fringe rate f_t (coordinate conjugate to the time) by the relation

$$k\theta_x = r/[(R-r)V_x]2\pi f_t. \tag{A15}$$

Replacing θ_x by f_t in equation (A12), we obtain

$$M_u(\tau, f_t) = \frac{r}{(R-r)V_x}\int {\rm d}\Delta f \times \int {\rm d}t \exp(-2\pi i(\Delta f\tau + f_t))\, B_u(\Delta f, \rho_x) \approx \frac{1}{2}\frac{R-r}{r}V_x\delta(\tau - af_t^2)\,\Phi_{S,1}\left(\frac{2\pi f_t r}{(R-r)V_x}\right), \tag{A16}$$

where

$$a = \lambda^2 Rr/[2(R-r)cV_x^2] \tag{A17}$$

is the arc curvature parameter. It is the same as defined in Stinebring et al. (2001) and Cordes et al. (2006).

We considered the case when unperturbed emission (spherically symmetric wave) falls on the phase screen with 1D inhomogeneities. There is also another model that deserves to be considered. Suppose that strongly scattering layer of turbulent plasma exists close to the pulsar. When the emission scattered in this layer reaches the main phase screen, the averaged power in the SS will be distributed inside the strip along the line $\tau = af_t^2$. We assume fluctuations of emission are defined by strong scintillation. The characteristic width of this strip in the direction to the variable f_t is approximately equal to $\Delta f_t \approx 1/2\pi t_0$, where t_0 is the characteristic correlation time of strongly perturbed radiation. Therefore, the contrast of the SS in this case is reduced, but individual arcs still may be distinguished.

This paper has been typeset from a Microsoft Word file prepared by the author.